Molecular dynamics simulation of the liquid–vapor interface: The Lennard-Jones fluid

Matthias Mecke and Jochen Winkelmann[a)]
Institut für Physikalische Chemie, Universität Halle-Wittenberg, Geusaer Str., D-06217 Merseburg, Germany

Johann Fischer
Institut für Land-, Umwelt-, und Energietechnik, Universität für Bodenkultur, Peter-Jordan-Strasse 82, A-1190 Wien, Austria

(Received 18 June 1997; accepted 20 August 1997)

In this work we present new molecular dynamics simulation results for the liquid–vapor interface of the pure Lennard-Jones fluid. Our aims were further investigations on the simulation setup and the simulation parameters to obtain reliable data for the coexisting densities as well as for the surface tension. The influence of the cut-off distance to the interfacial properties is investigated and long-range corrections to both the dynamics and the surface tension are applied. It is found that the saturated liquid densities from the surface simulations agree with those from the $NpT+$ test particle method within 1% for sufficiently large simulation boxes; the saturated vapor densities agree within 4%. In order to obtain reliable values for the surface tension, cut-off radii of at least 5 molecular diameters supplemented by a tail correction are required. © *1997 American Institute of Physics.* [S0021-9606(97)51044-0]

I. INTRODUCTION

Due to their fundamental importance for many technological processes, liquid–vapor and liquid–liquid interfaces have been a matter of great interest in several experimental and theoretical investigations. In the last decade, computer simulations became more and more an important tool to obtain information on the properties of pure homogeneous fluids and mixtures as well as on their interfacial behavior.

The primary results of a study on the liquid–vapor interface are the coexisting liquid and vapor densities. Several different approaches have been developed to obtain these properties from computer simulations like the Gibbs ensemble Monte Carlo method[1–3] or the $NpT+$ test particle method.[4] It was shown that these methods are able to reproduce the experimental phase equilibrium data of simple liquids and their mixtures with good accuracy.[5,6] However, these simulation techniques cannot yield information on the interfacial region itself, like microscopic structure, interfacial thickness, or such important quantities as surface tension or surface segregation for mixtures. Since there is no experimental technique to directly detect the microscopic interfacial structure, simulations of the two coexisting phases within one simulation cell were thought to be a useful tool to investigate these properties. Since this method was first applied to atomic fluids in 1974, several simulations have been reported for the liquid–vapor interface of the Lennard-Jones fluid using molecular dynamics or Monte Carlo techniques.[7–18] Although in principle these simulations use the same basic techniques as those well known for the simulation of bulk fluids, there are quite different ideas of how to set up and run the simulations. It turned out that not all of these approaches were suitable to produce consistent results. Furthermore, the direct liquid–vapor simulations require larger systems and significantly longer equilibration and production runs to stabilize the interface than those commonly used in bulk fluid simulations. Some of the earlier studies could not meet these requirements. Therefore, we find a considerable variation of results, especially for the surface tension caused by problems in the simulation setup or by insufficient simulation time.

Considering these findings, we see that the right choice of the simulation conditions and parameters is of fundamental importance for obtaining accurate results. Recently, Holcomb *et al.*[17] presented an excellent investigation on these problems and claimed the possibility of obtaining accurate surface tension results for the full Lennard-Jones potential from simulations with a moderate cut-off value by applying a tail correction. In a subsequent paper,[19] however, the original tail corrections were revised, and as a consequence the surface tension results obtained with the cut-off radii $r_c=4.4\sigma$ and $r_c=6.3\sigma$ show discrepancies of 4%. Moreover, the saturated liquid densities obtained with $r_c=4.4\sigma$ show discrepancies with respect to the $NpT+$ test particle results of Lotfi *et al.*[5] between 1.1% and 4.3%. Hence, we thought it worthwhile to reinvestigate the problem by using long-range corrections already to the dynamics, by using a more direct tail correction for the surface tension and by using somewhat larger cut-off radii.

II. SIMULATION TECHNIQUE

We used the molecular dynamics method to simulate a three-dimensional liquid in equilibrium with its own vapor. The molecules interact via a Lennard-Jones 12-6 potential with the parameters ε and σ. Consequently, we can denote all quantities in units reduced to these parameters. In particular, we define the reduced temperature $T^*=kT/\varepsilon$, the re-

a)Author to whom correspondence should be addressed.

 0021-9606/97/107(21)/9264/7/$10.00

duced length $z^*=z/\sigma$, the reduced density $\rho^*=\rho/\sigma^3$, and the reduced surface tension $\gamma^*=\gamma\sigma^2/\varepsilon$. The asterisk is omitted if no confusion can occur.

Our simulations were performed in a NVT ensemble, i.e., at prescribed particle number, volume, and temperature with different cut-off radii r_c. The temperature was kept constant by the momentum scaling method and the equations of motion were solved using a fifth-order predictor-corrector algorithm. The reduced time step Δt^* was varied from 0.002 to 0.005 in units of $\sigma\sqrt{m/\varepsilon}$. We will give the respective time step, as well as the total number of time steps and the cut-off radius used for each simulation run together with the results.

The simulation procedure was started from a face-centered-cubic (fcc) lattice in a cubic box. We chose a density slightly higher than the appropriate liquid density, which was available from our equation of state.[20] This choice causes the liquid film to have approximately the thickness of the cubic start box. After a short melting and equilibration period of this homogeneous phase, two empty cubic cells of the same dimensions were added to both sides of the film in the z-direction, allowing the vapor phase to develop. Then another equilibration stage of the liquid–vapor system followed to stabilize the interface. After the interfacial system was equilibrated the production period was performed, during which the coexisting densities and the surface tension were evaluated. The block average method[21] was used to estimate the statistical uncertainties of the computed surface tension values. Since the coexisting densities are determined from the final density profile by taking the mean liquid and gas densities under exclusion of the direct interfacial areas and the areas close to the vapor cell borders, we do not try to give statistical uncertainties for these properties, even though we can state that the density profile does not change considerably once a system is equilibrated. Therefore, we estimate the fluctuations in the coexisting densities to be rather small.

We applied periodic boundary conditions in the x-y-plane. In the z-direction one can use either periodic boundary conditions or hard reflecting walls. Although the hard wall model might seem to be a more realistic approach, it is more difficult to handle. Collisions of vapor phase particles with the hard wall induce an additional momentum, which, especially at higher temperatures, can cause the center of mass to move strongly. These movements have to be corrected by allowing the reference frame to move under attention to particles close to the walls. Running the simulation with complete periodic boundary conditions we only observe a negligible displacement of the center of mass, which, if necessary, can easily be corrected. Furthermore, the collision of a particle with the wall in the presence of another force within its cut-off radius is not exactly calculable by means of a predictor-corrector algorithm. However, we have performed both, simulations with complete periodic boundary conditions and simulations with the hard wall model, respectively, and we found no significant differences, neither in the density profiles nor in the surface tension results.

In our simulations we use a truncated potential, which means that the forces on a particle i from all particles within its cut-off sphere are computed exactly. In the case of a homogeneous fluid we can assume that the forces affecting this particle i from outside its cut-off sphere will average out and, therefore, have no influence on its trajectory. For an inhomogeneous fluid, this assumption is no longer valid. Particles close to the liquid–gas interface especially feel an additional attractive force from the liquid slab outside of their truncation spheres. This additional force has to be taken into consideration when solving the equations of motion in the simulation of inhomogeneous fluids. Lotfi *et al.*[22] were the first to apply such long-range corrections to molecular dynamics simulations, and describe the additional force ΔF affecting a particle i as

$$\Delta F=-\frac{d(\Delta u)}{dr}, \tag{1}$$

with

$$\Delta u=\int_{r_{ij}>r_c} u_{ij}(r_{ij})\rho(r_j)dr_{ij}. \tag{2}$$

Considering a Lennard-Jones fluid with inhomogeneity in the z-direction, we obtain

$$\Delta F_z/8\pi=-\int_{-\infty}^{-r_c} dz_{ij}\rho(z_j)(z_{ij}^{-11}-z_{ij}^{-5}) - \int_{r_c}^{\infty} dz_{ij}\rho(z_j)(z_{ij}^{-11}-z_{ij}^{-5}), \tag{3}$$

using cylindrical coordinates. The local density $\rho(z)$ can be obtained either from a step function or directly from the density profile computed within the simulation.

We included this ansatz in our simulation algorithm and used for $\rho(z)$ the density profile computed within the simulation. At the very beginning of the production phase we applied the final profile from the equilibration run for the first 5000 time steps.

III. DENSITY PROFILES

The first result we obtain from our liquid–vapor surface simulations is the density profile. It is determined by dividing the simulation cell in a certain number of slabs in the z-direction and taking the number of particles in each one. In our simulations we used 300 to 600 slabs, depending on the box geometries. The slab densities are accumulated and averaged over the production run to yield the final profile. It turned out that a balanced density profile can already be obtained very soon, usually after 10 000 to 20 000 time steps, while longer runs are required to calculate the surface tension accurately.

Typical profiles at three temperatures are shown in Figs. 1–3. We performed simulations with a cut-off distance $r_c=2.5\sigma$ and $r_c=5.0\sigma$, each with and without long-range corrections to the dynamics (LRC), in order to investigate its influence on the density profile and on the coexisting densities. We learn from Figs. 1–3 that the profiles determined by $r_c=2.5\sigma$ simulations are rather flat. They show lower liquid and higher vapor densities and a larger interfacial thickness than those profiles at higher cutoff. We find the long-range

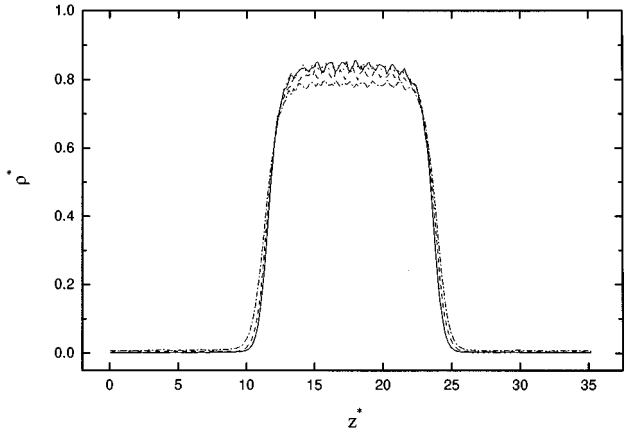

FIG. 1. Density profiles for the reduced temperature $T^*=0.70$ obtained from simulations with $r_c=2.5\sigma$ and no LRC (–·–·–), with $r_c=2.5\sigma$ and LRC (– – –), with $r_c=5.0\sigma$ and no LRC (·····), and with $r_c=5.0\sigma$ and LRC (—).

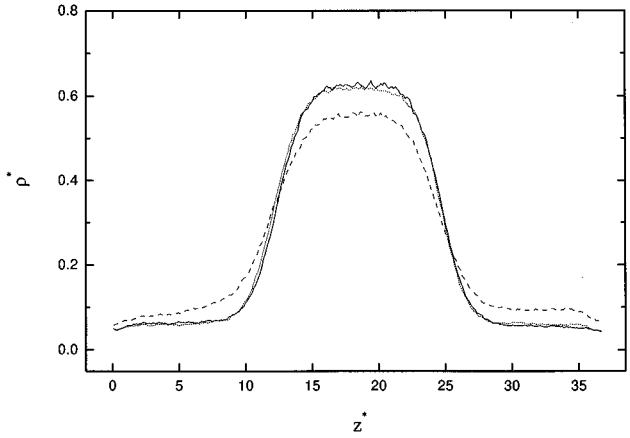

FIG. 3. Density profiles for the reduced temperature $T^*=1.10$ obtained from simulations with $r_c=2.5\sigma$ and LRC (– – –), with $r_c=5.0\sigma$ and no LRC (·····), and with $r_c=5.0\sigma$ and LRC (—). The simulation with $r_c=2.5\sigma$ and no LRC could not yield a sharp density profile.

corrections working quite well, even though they are, especially at high temperatures, not able to correct this behavior completely. In the case of the profiles obtained from $r_c=5.0\sigma$ simulations we can hardly see an influence of the long-range corrections at the two lower temperatures. Only at the highest temperature the use of long-range corrections causes a slightly better profile.

In Table I we summarize the corresponding results for the orthobaric densities determined from these profiles. The values confirm the behavior we have seen in the figures. Additional simulations with $r_c=6.5\sigma$ and LRC did not show relevant changes in the density profiles and the orthobaric densities.

In the upper part of Table II we compare our most reliable results for the orthobaric densities from Table I ($r_c=5.0\sigma$, LRC) with the results of Lotfi *et al.*,[22] also obtained from direct liquid–vapor interface simulations using long-range corrections to the dynamics. We find that the agreement between both data sets is good. In Table II we additionally include the results of Lotfi *et al.*[5] for the coexisting densities determined by the $NpT+$test particle method. This method is known to yield very reliable and exact results for these properties. Therefore, these data can be used as a test for the accuracy of our procedure. Although the direct liquid–vapor simulation is not able to reach the accuracy of the $NpT+$test particle method, we see that at the two lower temperatures the values for the coexisting densities are quite close to those from the $NpT+$test particle method. The difference in the liquid densities, for instance, is less than 1%. Only for the reduced temperature $T^*=1.10$ we find a considerable discrepancy. To find out whether the deviation vanishes if we further improve the simulation conditions, we modified the box geometry toward a thicker liquid film by duplicating the simulation cell in the z-direction. The results are shown in the lower part of Table II. The liquid density resulting from this simulation agrees now within 0.4% with the $NpT+$test particle result. So we can state that even at high temperature the direct liquid–vapor simulation

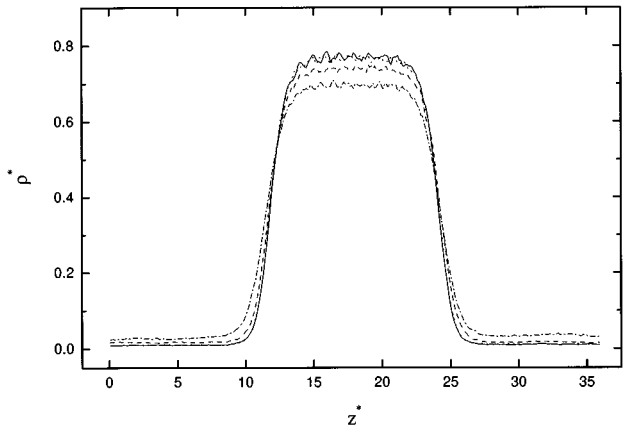

FIG. 2. Density profiles for the reduced temperature $T^*=0.85$ obtained from simulations with $r_c=2.5\sigma$ and no LRC (–·–·–), with $r_c=2.5\sigma$ and LRC (– – –), with $r_c=5.0\sigma$ and no LRC (·····), and with $r_c=5.0\sigma$ and LRC (—).

TABLE I. Simulation results for the orthobaric densities obtained from different simulation conditions. $N=1372$, equil. steps$=50\,000$, prod. steps $=200\,000$, $\Delta t^*=0.002$.

T^*	r_c^*	LRC	ρ_{liq}^*	ρ_{gas}^*
0.70	2.5	no LRC	0.7861	0.007 84
0.70	2.5	LRC	0.8154	0.004 84
0.70	5.0	no LRC	0.8360	0.001 94
0.70	5.0	LRC	0.8375	0.002 01
0.85	2.5	no LRC	0.6956	0.030 25
0.85	2.5	LRC	0.7391	0.016 53
0.85	5.0	no LRC	0.7659	0.010 41
0.85	5.0	LRC	0.7698	0.009 77
1.10	2.5	no LRC		
1.10	2.5	LRC	0.5546	0.090 32
1.10	5.0	no LRC	0.6169	0.059 57
1.10	5.0	LRC	0.6236	0.059 37

TABLE II. Results for the orthobaric densities obtained from the present simulations in comparison with the results from direct surface simulations of Lotfi *et al.* (Ref. 22) and the $NpT+$test particle simulations of Lotfi *et al.* (Ref. 5).

		This work		Lotfi *et al.* (Ref. 22)		$NpT+$test particle (Ref. 5)	
T^*	Box dimension $x^*\times z^*$	ρ^*_{liq}	ρ^*_{gas}	ρ^*_{liq}	ρ^*_{gas}	ρ^*_{liq}	ρ^*_{gas}
0.70[a]	11.75×35.25	0.8375	0.002 01	0.8403	0.002 13	0.8427	0.001 93
0.85[a]	11.99×35.97	0.7698	0.009 77	0.7715	0.008 90	0.7762	0.009 70
1.10[a]	12.25×36.75	0.6236	0.059 37	0.6270	0.0572	0.6401	0.053 30
1.10[b]	12.25×73.50	0.6378	0.055 28	0.6270	0.0572	0.6401	0.053 30

[a]$N=1372$, $r_c=5.0\sigma$, LRC, equil. steps=50 000, prod. steps=200 000, $\Delta t^*=0.002$.
[b]$N=2744$, $r_c=6.124\sigma$, no LRC, equil. steps=80 000, prod. steps=50 000, $\Delta t^*=0.003$.

method is able to determine the coexisting densities with good accuracy.

IV. SURFACE TENSION

A. Results without tail correction

The surface tension was calculated during the simulation by means of the virial expression[16,23,24]

$$\gamma=\frac{1}{2A}\left\langle \sum_{\substack{i<j\\ r<r_c}} \left(r_{ij}-\frac{3z_{ij}^2}{r_{ij}}\right)u'(r_{ij})\right\rangle, \tag{4}$$

where A is the total surface area $A=2xy$. The prime denotes differentiation and the angle brackets refer to a time average. The summation extends over all particles within the cut-off radius.

In Table III we give the surface tension values obtained from our simulations for different temperatures and cut-off distances. As long as no tail correction is applied to Eq. (4), this equation obviously requires an increase of γ with r_c. In Fig. 4 we compare our results with the most recent results of Holcomb *et al.*[17] Considering the cut-off distances which were used in the simulations we find both data sets to be consistent with each other. We have to note that in contrast to the values of Holcomb *et al.* our results were determined using long-range corrections to the dynamics. As these corrections decrease the interfacial thickness for simulations with small cut-off radius they also affect the surface tension. This behavior can be observed for the $r_c=2.5\sigma$ values.

TABLE III. Simulation results for the surface tension and the tail correction term to these results determined by the method of Blokhuis *et al.* (Ref. 19), Eqs. (6) and (7), and by the new method, Eqs. (8) and (10), described in this work.

T^*	r_c^*	γ^*	γ^*_{tail} method (Ref. 19)	γ^*_{tail} new method	$\gamma^*+\gamma^*_{tail}$ (γ^*_{tail} new method)
0.70[a]	2.5	0.6509±0.0196	0.4183	0.4080	1.0589
0.70[a]	5.0	1.0217±0.0193	0.1245	0.1177	1.1394
0.70[b]	6.5	1.0753±0.0194	0.0757	0.0699	1.1452
0.85[a]	2.5	0.3922±0.0157	0.2986	0.2933	0.6855
0.85[a]	5.0	0.6983±0.0172	0.0995	0.0944	0.7927
0.85[b]	6.5	0.7527±0.0162	0.0606	0.0569	0.8096
1.10[a]	2.5	0.0935±0.0113	0.0839	0.0862	0.1797
1.10[a]	5.0	0.2721±0.0139	0.0497	0.0472	0.3193
1.10[b]	6.5	0.2853±0.0122	0.0318	0.0297	0.3150

[a]$N=1372$, LRC, equil. steps=50 000, prod. steps=200 000, $\Delta t^*=0.002$.
[b]$N=2048$, LRC, equil. steps=50 000, prod. steps=200 000, $\Delta t^*=0.002$.

B. Tail correction procedures

Since we calculate the surface tension from Eq. (4) considering only the interactions within the cut-off sphere, we need a tail correction term γ_{tail} which enables us to estimate the surface tension for the full Lennard-Jones potential. This term represents the contribution of the potential for distances larger than r_c to the surface tension. For the determination of γ_{tail}, Salomons and Mareschal[16,25] used a formula according to Fowler[26]

$$\gamma_{tail}=\tfrac{3}{2}\,\pi(\rho_{liq}/r_c)^2. \tag{5}$$

For the simulated liquid–vapor systems this is a very simplified expression, since this formula includes the assumption that the transition layer has zero thickness and that $\rho(z)$ has a constant value ρ_{liq} on the liquid side of the dividing surface and $\rho_{gas}=0$ on the gas side. A more realistic ansatz was given by Chapela *et al.*,[9] later corrected by Blokhuis *et al.*[19]

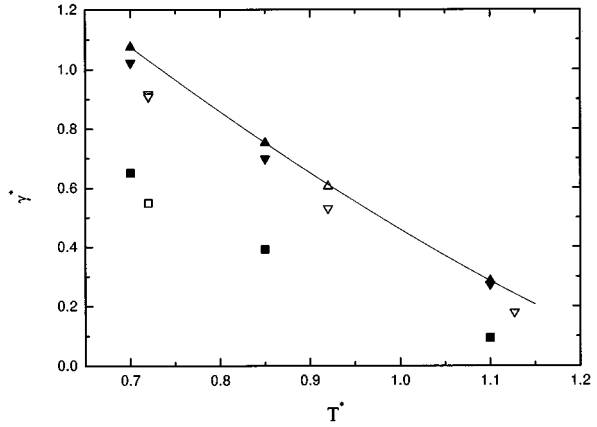

FIG. 4. Results for the reduced surface tension γ^* without tail correction versus the reduced temperature obtained from simulations with $r_c=2.5\sigma$ (■), with $r_c=5.0\sigma$ (▼), and with $r_c=6.5\sigma$ (▲) of this work, in comparison with those obtained from simulations with $r_c=2.5\sigma$ (□), with $r_c=4.4\sigma$ (▽), and with $r_c=6.3\sigma$ (△) of Holcomb *et al.* (Ref. 17). The line connecting the $r_c=6.5\sigma$ data is a guide to the eye.

$$\gamma_{\text{tail}} = 12\pi(\rho_{\text{liq}} - \rho_{\text{gas}})^2 \int_0^1 ds \int_{r_c}^{\infty} dr\ r^{-3}(3s^3 - s)\coth\left(\frac{2sr}{\xi}\right), \tag{6}$$

where ξ is the interfacial thickness obtained from fitting the final density profile by an expression

$$\rho(z) = \tfrac{1}{2}(\rho_{\text{liq}} + \rho_{\text{gas}}) - \tfrac{1}{2}(\rho_{\text{liq}} - \rho_{\text{gas}})\tanh\left(\frac{2(z - z_0)}{\xi}\right). \tag{7}$$

We will confirm below that Eq. (6) in combination with Eq. (7) works quite well for pure fluids. We have, however, problems in extending Eq. (6) to mixtures because the partial density profiles need not follow a tanh-function.

Hence, we suggest here a more direct procedure and calculate an individual tail contribution γ_i^{tail} for each particle i at each time step within the simulation run, and form the average

$$\gamma_{\text{tail}} = \frac{1}{2A}\left\langle \sum_{\substack{i \\ r > r_c}} \gamma_i^{\text{tail}} \right\rangle. \tag{8}$$

In order to determine the individual tail contribution γ_i^{tail}, we start again at the virial route formula given by Eq. (4) and apply it to the interactions of a particle i in the simulation box with all particles j outside its cut-off sphere in an infinite volume. Using the density profile, the single particles j can now be replaced by the estimated number of these particles in a volume element dV. Using spherical coordinates we obtain a tail contribution for each particle i,

$$\gamma_i^{\text{tail}} = \frac{1}{2}\int_{r=r_c}^{\infty} dr \int_0^{\pi} d\vartheta \int_0^{2\pi} d\varphi \times\left(r - \frac{3z^2}{r}\right)\rho(r)u'(r)r^2 \sin\vartheta. \tag{9}$$

Dividing by 2 in Eq. (9) is to avoid double counting. Since the system is inhomogeneous only in the z-direction, the integration over φ can be performed to yield

$$\gamma_i^{\text{tail}} = \pi\int_{r=r_c}^{\infty} dr \int_0^{\pi} d\vartheta r^3(1 - 3\cos^2\vartheta)u'(r) \times\rho(z_i + r\cos\vartheta)\sin\vartheta. \tag{10}$$

We want to emphasize that Eq. (10) uses the actual density profile obtained within the simulation and does not require any prescribed functional form.

We found $\Delta r = 0.05\sigma$ and $\Delta\vartheta = \pi/200$ to be sufficient to perform the numerical integration with very good accuracy. The integration over r was performed from $r = r_c$ to $r = 50\sigma$. For computational reasons it is not possible to carry out the integration procedure for each particle at each time step. But we can use the fact that γ_i^{tail} only depends on the position of particle i in the z-direction. So we can divide the simulation box in small intervals Δz and compute $\gamma^{\text{tail}}(z)$ for each of these elements. Since the density profile does not change considerably for a system, once equilibrated it is sufficient to bring the values up to date every some thousand time steps. Then a particle i is associated with its volume element Δz according to its current position at each time step. Applying this technique, our simulations took only negligibly longer than comparable runs without tail correction calculation.

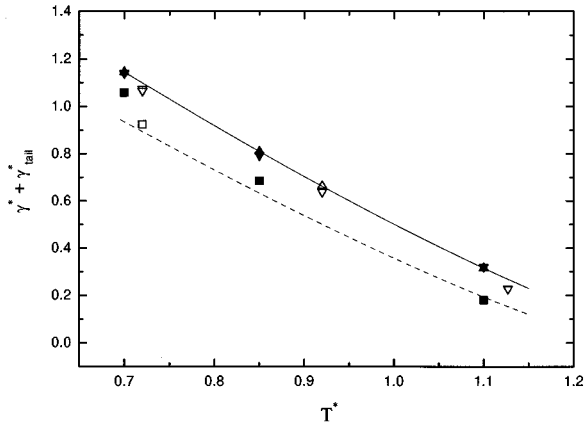

FIG. 5. Results for the reduced surface tension with tail correction $\gamma^* + \gamma_{\text{tail}}^*$ versus the reduced temperature obtained from simulations with $r_c = 2.5\sigma$ (■), with $r_c = 5.0\sigma$ (▼), and with $r_c = 6.5\sigma$ (▲) of this work, in comparison with those obtained from simulations with $r_c = 2.5\sigma$ (□), with $r_c = 4.4\sigma$ (▽), and with $r_c = 6.3\sigma$ (△) of Holcomb *et al.* (Ref. 17). The line connecting the $r_c = 6.5\sigma$ data is the correlation function given by Eq. (11). The broken line shows the experimental results for krypton.

C. Results with tail correction

Table III shows the surface tension γ^* without tail correction obtained from our simulations, and its tail correction term γ_{tail}^* determined by the method of Blokhuis *et al.*,[19] Eqs. (6) and (7), on the one hand, and by our new method, Eqs. (8) and (10), on the other. First, we find good agreement between both tail corrections.

We concentrate now on the sum $\gamma^* + \gamma_{\text{tail}}^*$ given in the last column of Table III. We observe that for the cut-off radius $r_c = 2.5\sigma$ the tail corrected surface tensions differ appreciably from the values obtained with the higher cut-off radii. Two reasons are responsible for this behavior. On the one hand, we know from Figs. 1–3 that the density profiles obtained for $r_c = 2.5\sigma$, even with LRC, differ from the profiles for higher cut-off radii. On the other hand, the tail corrections assume the pair correlation function to be unity for intermolecular distances larger than r_c; while for homogeneous fluids, deviations of $g(r)$ from 1 seem to compensate already for rather small cut-off radii, we cannot expect the same behavior in the case of strong density gradients.

Let us consider now the results obtained with the cut-off radii $r_c = 5.0\sigma$ and $r_c = 6.5\sigma$. The largest discrepancy occurs at the medium temperature and amounts to 2%; the discrepancy is, however, within the simulation uncertainty of each simulation.

As we have now surface tensions obtained with the rather large cut-off radius $r_c = 6.5\sigma$ at three temperatures, we

thought it to be of interest for further comparisons to derive a correlation equation in the form

$$\gamma^* + \gamma^*_{\text{tail}} = A[1 - T/T_R]^b. \tag{11}$$

Using the $\gamma^* + \gamma^*_{\text{tail}}$ values from Table III we obtain $A = 2.960\,19$, $T_R = 1.325\,21$, and $b = 1.264\,15$. We have to mention that T_R should be the critical temperature. As a matter of fact, the present T_R-value lies between the previous estimate of Lotfi *et al.*,[5] $T_c = 1.314$, and the estimate of Mecke *et al.*,[20] $T_c = 1.328$. From correlations of experimental surface tension data, b is known to be about 11/9,[27] and hence, our b-value is also quite reasonable.

A comparison of our data with those of Holcomb *et al.*[17] is given in Fig. 5. Please note that the tail contribution originally published by Holcomb *et al.*[17] is not correct, as they used the old objectionable ansatz of Chapela *et al.*[9] We include the corrected values obtained by Blokhuis *et al.*[19] We see that the one result of Holcomb *et al.* obtained with $r_c = 6.3\sigma$ is in perfect agreement with our correlation function. The $r_c = 4.4\sigma$ results, however, show some deviations from the correlation function which can be attributed to the reasons discussed already for the 2.5σ cut-off radius. At $T^* = 1.127$, in particular, the density profile of Holcomb *et al.* must have some deficiency, as the saturated liquid density differs from the $NpT+$ test particle result by 4.3%, which in turn seems to influence the surface tension. We learn from these studies that the surface tension results converge to a theoretical value of the full Lennard-Jones potential which can be estimated by simulations with a cut-off radius of at least 5σ and a tail correction term.

Finally, Fig. 5 contains also experimental results for krypton[28–31] reduced with the parameters $\sigma = 0.3638$ nm and $\epsilon/k = 166.7$ K.[32] The remarkable discrepancy is attributed to the fact that the Lennard-Jones potential can be considered only as an effective pair potential, while in nature three-body and higher many-body potentials are present which become important in the case of density gradients. Moreover, one could discuss capillary waves widening the interface and, therefore, decreasing the surface tension.

D. Effects of the box geometry

So far, all the simulations for the surface tension were performed with the simulation box $z = 3x = 3y$ as described in Sec. II. Now it it interesting to see whether the surface tension values are sensitive to changes in the box geometry. The idea was to set up a simulation cell with a thicker liquid film and a larger gas volume. For that purpose we duplicated the simulation cell in the z-direction to yield a cell with the dimensions $z = 6x = 6y$. Using such a system, we are absolutely sure that no particle in the liquid film can realize any influence from both surfaces at the same time within its cut-off radius. The results are given in Table IV. Comparing the values for $\gamma^* + \gamma^*_{\text{tail}}$ we see that there is no significant difference to the ones obtained with the usual cell geometry.

TABLE IV. Surface tension obtained from simulations with different box dimension. $N = 2744$, no LRC, equil. steps = 80 000, prod. steps = 50 000, $\Delta t^* = 0.003$.

T^*	r_c^*	Box dimension $x^* \times z^*$	γ^*	γ^*_{tail}	$\gamma^* + \gamma^*_{\text{tail}}$
0.70	5.873	11.75×70.50	1.0523 ± 0.0496	0.0922	1.1445
0.85	5.996	11.99×71.94	0.7446 ± 0.0416	0.0716	0.8162
1.10	6.124	12.25×73.50	0.2792 ± 0.0306	0.0365	0.3157

V. CONCLUSION

We have performed molecular dynamics simulations to investigate the liquid–vapor interfacial properties of the Lennard-Jones fluid. We have simulated a three-dimensional liquid film in equilibrium with its vapor to obtain information on the density profiles, the orthobaric densities, and the surface tension. In order to consider the influence of the cut-off radius to the results, long-range corrections to the dynamics and the surface tension have been tested and applied.

Using sufficiently large simulation systems the surface simulations yield coexisting densities which agree with those from the $NpT+$ test particle method within 1% for the liquid and 4% for the vapor side. The surface tension results converge to a theoretical value of the full Lennard-Jones potential, which can be estimated by simulations with a cut-off radius of at least 5σ and a tail correction term. Moreover, at higher temperatures the simulation box must be sufficiently large to allow the formation of a liquid slab with constant density.

ACKNOWLEDGMENT

This work was supported by the Deutsche Forschungsgemeinschaft, Az, Wi 1081/7-1.

[1] A. Z. Panagiotopoulos, Mol. Phys. **61**, 813 (1987).
[2] A. Z. Panagiotopoulos, Mol. Simul. **9**, 1 (1992).
[3] A. Z. Panagiotopoulos, N. Quirke, M. Stapleton, and D. J. Tildesley, Mol. Phys. **63**, 527 (1988).
[4] D. Möller and J. Fischer, Mol. Phys. **69**, 463 (1990); **75**, 1461 (1992).
[5] A. Lotfi, J. Vrabec, and J. Fischer, Mol. Phys. **76**, 1319 (1992).
[6] J. Vrabec and J. Fischer, AIChE J. **43**, 212 (1997).
[7] K. S. Liu, J. Chem. Phys. **60**, 4226 (1974).
[8] J. K. Lee, J. A. Barker, and G. M. Pound, J. Chem. Phys. **60**, 1976 (1974).
[9] G. A. Chapela, G. Saville, and J. S. Rowlinson, Faraday Discuss. Chem. Soc. **59**, 22 (1975); G. A. Chapela, G. Saville, S. M. Thompson, and J. S. Rowlinson, J. Chem. Soc. Faraday Trans. 2 **73**, 1133 (1977).
[10] J. Miyazaki, J. A. Barker, and G. M. Pound, J. Chem. Phys. **64**, 3364 (1976).
[11] M. Rao and D. Levesque, J. Chem. Phys. **65**, 3233 (1976).
[12] M. Rao and B. J. Berne, Mol. Phys. **37**, 455 (1979).
[13] J. P. R. B. Walton, D. J. Tildesley, and J. S. Rowlinson, Mol. Phys. **48**, 1357 (1983).
[14] M. Matsumoto and Y. Kataoka, J. Chem. Phys. **88**, 3233 (1988).
[15] M. J. P. Nijmeijer, A. F. Bakker, C. Bruin, and J. H. Sikkenk, J. Chem. Phys. **89**, 3789 (1988).
[16] E. Salomons and M. Mareschal, J. Phys.: Condens. Matter **3**, 3645 (1991).
[17] C. D. Holcomb, P. Clancy, S. M. Thompson, and J. A. Zollweg, Fluid Phase Equilibria **75**, 185 (1992); **88**, 303 (1993); C. D. Holcomb, P. Clancy, and J. A. Zollweg, Mol. Phys. **78**, 437 (1993).
[18] L. Chen, J. Chem. Phys. **103**, 10,214 (1995).
[19] E. M. Blokhuis, D. Bedeaux, C. D. Holcomb, and J. A. Zollweg, Mol. Phys. **85**, 665 (1995).

[20] M. Mecke, A. Müller, J. Winkelmann, J. Vrabec, J. Fischer, R. Span, and W. Wagner, Int. J. Thermophys. **17**, 391 (1996).
[21] D. Fincham, N. Quirke, and D. J. Tildesley, J. Chem. Phys. **84**, 4535 (1986).
[22] A. Lotfi, J. Vrabec, and J. Fischer, Mol. Simul. **5**, 233 (1990).
[23] J. S. Rowlinson and B. Widom, *Molecular Theory of Capillarity* (Clarendon, Oxford, 1982).
[24] J. G. Kirkwood and F. P. Buff, J. Chem. Phys. **17**, 338 (1949).
[25] E. Salomons and M. Mareschal, J. Phys.: Condens. Matter **3**, 9215 (1991).
[26] R. H. Fowler, Proc. R. Soc. London, Ser. A **159**, 229 (1937).
[27] O. Redlich, *Thermodynamics: Fundamentals, Applications* (Elsevier, Amsterdam, 1976).
[28] V. A. M. Soares, B. S. Almeida, I. A. McLure, and R. A. Higgins, Fluid Phase Equilibria **32**, 9 (1986).
[29] B. S. Almeida, V. A. M. Soares, I. A. McLure, and J. C. G. Calado, J. Chem. Soc. Faraday Trans. 1, **85**(6), 1217 (1989).
[30] C. D. Holcomb and J. A. Zollweg, Fluid Phase Equilibria **75**, 213 (1992).
[31] I. I. Sulla and V. G. Baidakov, Zh. Fiz. Khim. **68**, 63 (1994).
[32] K. C. Nadler, J. A. Zollweg, W. B. Streett, and I. A. McLure, J. Colloid Interface Sci. **122**, 530 (1988).